Deformation Analysis of Induction Machines by Means of Analytical and Numerical Methods

Christoph Schlensok[1], Dirk van Riesen[2], Michael van der Giet[2], and Kay Hameyer[2]

[1]Bosch Rexroth AG, D-97816 Lohr am Main, Germany
[2]Institute of Electrical Machines, RWTH Aachen University, D-52062 Aachen, Germany

The estimation and calculation of the acoustic sound of electric machinery is of high interest. Various approaches have been presented relying either on analytical or on numerical models. In general, the analytical models are based on the electromagnetic-field theory, and the results are compared to measurements. Numerical models allow for the separation of different exciting forces stemming from various effects. In the studied case of an induction machine (IM) with squirrel-cage rotor the three following effects are taken into account in the analytical model: the fundamental field, saturation, and eccentricity. Nevertheless, the numerical results have to be verified. Hence, they are compared to the physically based analytical results. The radiated noise depends directly on the surface's deformation of the machine. Therefore, the analysis is focused on the structure-dynamic vibrations. The combined analysis presented here, allows for the reduction of vibrations and noise optimizing the coupling of stator and housing. The studied IM's housing is mounted with six spiral-steel springs to the stator. With the presented method the impact of different numbers of pins is analyzed.

Index Terms—**Audible noise, deformation, finite-element methods, induction machine (IM), structure dynamics, vibrations.**

I. Introduction

THERE have been several contributions to both the analytical [1] and numerical [2], [3] approach of estimating the radiated noise of electrical machinery. A comparison as well as a combination of both methods allows for more reliable predictions and faster improvements of the machine's structure in the sense of a quiet machine.

In this paper an induction machine (IM) with a squirrel-cage rotor is studied by means of analytical and numerical methods. At first the applied models are introduced. In general, the structure of an IM is not purely cylindrical as the analytical models of [1] assume. Therefore, an add-on of the analytical model is presented. For comparison reasons different numerical finite-element (FE) models are introduced in a second step. Finally, the obtained results of both models are presented and analyzed.

II. Analytical Model

The analytical model [1] is based on the analysis of the radial force-waves F_{radial} resulting from the radial component of the air-gap flux-density B_n depending on space x and time t

$$F_{\mathrm{radial}}(x,t) = \frac{B_n^2(x,t)}{2\mu_0} \tag{1}$$

with μ_0 being the magnetic field constant. $B_n^2(x,t)$ results from the fundamental and harmonic field of the stator interacting with the induced fundamental and harmonic field of the rotor. Three major effects are considered in the analytical model: the fundamental air-gap field, the saturation of the lamination, and static and dynamic eccentricity. Each harmonic, i.e., each exciting force-wave frequency, results in oscillating space modes along the circumference of the stator at the air gap. The mode numbers r depend on the origin of the interacting field components of stator and rotor.

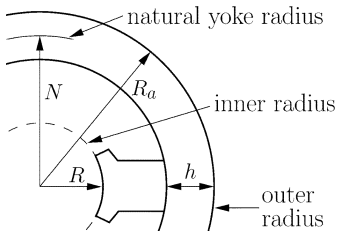

Fig. 1. Simplified analytical model of IM with teeth.

These force waves excite the structure of the machine, in particular stator and housing. The analytical model simplifies the machine's structure to a cylinder ring as Fig. 1 describes. In order to include the effect of slotting, the cylinder-ring model is modified taking the teeth into account introducing the adjusting factor

$$\Delta = \frac{\text{yoke weight}}{\text{tooth weight} + \text{yoke weight}}. \tag{2}$$

The weight of yoke and teeth is the equivalent to the corresponding cross sections. With Δ the eigenfrequency reads

$$F_0 = \frac{C_s}{2\pi \cdot N \cdot \sqrt{\Delta}}. \tag{3}$$

C_s is calculated taking the mass density ρ and Young's modulus E into account

$$C_s = \sqrt{\frac{E}{\rho}}. \tag{4}$$

With the analytical model the deformation magnitude of the analyzed oscillation mode r is estimated on the outer radius of the stator R_a. For this, the static and dynamic deformation factor is calculated for an adequate cylinder ring. Since $r = 0$ results in pure tensile stress the static deformation is calculated to

$$Y_{0,\mathrm{stat}} = \frac{R \cdot N}{E \cdot h} \cdot \sigma(f, r = 0) \tag{5}$$

Digital Object Identifier 10.1109/TMAG.2007.916498

TABLE I
STATIC DEFORMATION FACTORS FOR DIFFERENT MODES r

r	0	1	2	3	4	5	6
$\eta_{r,stat}$	1.0	596.4	35.7	5.0	1.4	0.6	0.3

with the natural yoke radius N, the height of the yoke h, and the inner radius of the stator R (see Fig. 1). The static deformation for mode number $r \geq 2$ is estimated with

$$Y_{r,\mathrm{stat}} = \frac{R \cdot N}{E \cdot h} \cdot \frac{\sigma}{i^2(r^2-1)^2} \qquad \text{for } r \geq 2 \tag{6}$$

$$i = \left(\frac{1}{2\sqrt{3}}\right) \cdot \left(\frac{h}{N}\right). \tag{7}$$

The static factor as ratio of $(Y_{r,\mathrm{stat}})/(Y_{0,\mathrm{stat}})$ reads

$$\eta_{r,\mathrm{stat}} = \frac{12}{(r^2-1)^2} \cdot \left(\frac{N}{h}\right)^2 \qquad \text{for } r \geq 2. \tag{8}$$

Bending forces are generated by $r = 1$. In this special case the corresponding static factor is calculated by

$$\eta_{1,\mathrm{stat}} = \frac{4}{3} \frac{h \cdot l_{\mathrm{Fe}}}{N \cdot \left(\frac{d}{L}\right)^4 \cdot L} \tag{9}$$

where l_{Fe} is the effective stack length and L the distance between both bearings. For $r \geq 1$ the factors given above are multiples of the deformation calculated for $r = 0$. Table I resumes the static deformation factors for the studied IM.

The relative sensitivity of the structure γ is defined as the ratio of the force-wave harmonic f_r and the eigenfrequency F_0. With this and the bending and longitudinal oscillation frequencies f_r^B and f_r^L respectively, the dynamic factor reads

$$\eta_{r,\mathrm{dynamic}} = \frac{r^2 - \gamma^2}{\left[\gamma^2 - \left(\frac{f_r^B}{F_0}\right)^2\right] \cdot \left[\gamma^2 - \left(\frac{f_r^L}{F_0}\right)^2\right]} \qquad \text{for } r \geq 2. \tag{10}$$

In the special case $r = 1$, the lowest bending eigenfrequency is of interest

$$F_{b1}'' = \frac{1}{2\pi} \sqrt{\frac{c_1''}{m''}}. \tag{11}$$

For a machine with the shaft diameter d the spring constant c_1'' reads

$$c_1'' = \frac{3\pi}{4} \cdot E \cdot \left(\frac{d}{L}\right)^4 \cdot L. \tag{12}$$

The adequate mass m'' is calculated by

$$m'' = \rho_{\mathrm{Fe}} \cdot 10^2 \cdot \left\{ l[(2R)^2 - d^2] + \frac{1}{2} \cdot L \cdot d^2 \right\} \tag{13}$$

with the mass density $\rho_{\mathrm{Fe}} = 7.8\,(\mathrm{kg})/(\mathrm{m}^3)$ of the rotor. Taking F_{b1}'' into consideration the dynamic deformation factor reads

$$\eta_1 = \frac{1}{1 - \gamma^2 \cdot \left(\frac{F_0}{F_{b1}''}\right)^2}. \tag{14}$$

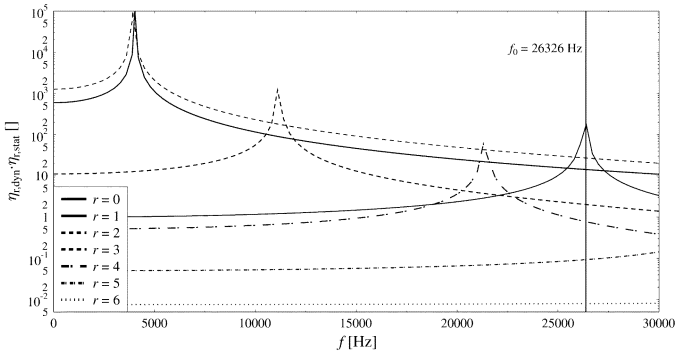

Fig. 2. Resulting factor $\eta_{\mathrm{stat}} \cdot \eta_{\mathrm{dyn}}(r)$.

Finally, the overall deformation magnitude is calculated by

$$Y_r = \eta_{r,\mathrm{stat}} \cdot \eta_{r,\mathrm{dynamic}} \cdot Y_{0,\mathrm{stat}}. \tag{15}$$

Fig. 2 shows the resulting behavior of the factor $\eta_{\mathrm{stat}} \cdot \eta_{\mathrm{dyn}}(r)$ for the studied IM. Each mode number r shows a resonance. Due to the small size of the regarded IM (800 W) these resonance frequencies are at high values. For $r \geq 4$ they are beyond the human ear's hearing ability. Next to this, the modes $r \geq 3$ produce small amplification factors throughout the spectrum. For the analysis of the studied machine, the spectrum is reduced to $f_{\max} = 2000$ Hz due to the application. Here, the modes r show approximately constant amplification factors for all frequencies. Therefore, the analysis of the deformation is reduced to small mode numbers $r \leq 10$. In case there are even two modes at the same frequency, the amplification factor decides, which of them is significant and which is negligible.

III. NUMERICAL MODEL

The finite-element model of the studied IM includes all mechanical parts of the machine (Fig. 3). The complex and detailed modelled structure of the IM does not correspond exactly to the analytical model introduced above (Fig. 1). Therefore, a more general and cylindrical model of the IM is applied first. By this, the numerical and analytical results can be compared and the models are verified. The simple model consists of the stator with winding and housing caps not considering the housing and the spiral-steel springs.

The numerical model provides the deformation for all nodes of the FE model. After discretization, the following oscillation equation is obtained [4]:

$$K \cdot D + C \cdot \dot{D} + M \cdot \ddot{D} = F. \tag{16}$$

K is the global stiffness matrix, D the vector of the total node displacement, C the damping matrix, M the mass matrix, and F the excitation force. By means of harmonic analysis, with $(d)/(dt) = j\omega$ and $(d^2)/(dt^2) = -\omega^2$ (16) becomes

$$(K + j\omega C - \omega^2 M) \cdot D = F. \tag{17}$$

The displacement of each single node included in D is defined by its displacement vector

$$\underline{u} = (\, u\ v\ w\,)^T. \tag{18}$$

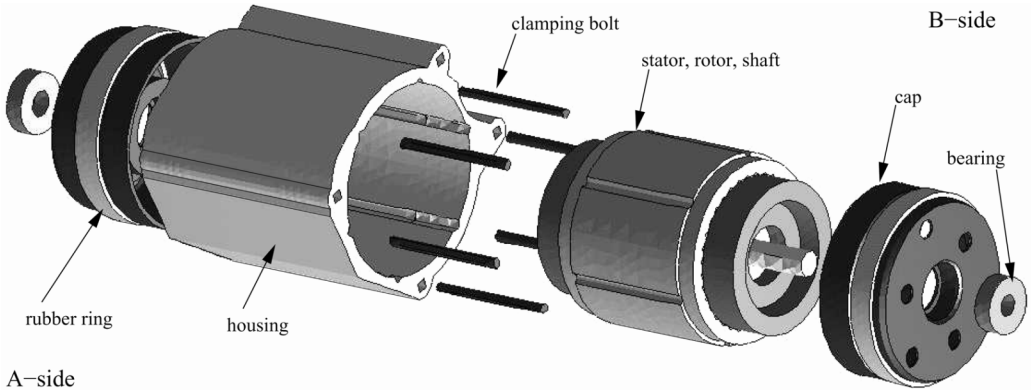

Fig. 3. Mechanical FE model (exploded view).

A body's strain $\underline{\epsilon}$ may be interpreted as the gradient of $\underline{u}$

$$\underline{\epsilon} = \begin{pmatrix} \epsilon_x \\ \epsilon_y \\ \epsilon_z \\ \gamma_{xy} \\ \gamma_{yz} \\ \gamma_{zx} \end{pmatrix} = \begin{bmatrix} \frac{\partial}{\partial x} & 0 & 0 \\ 0 & \frac{\partial}{\partial y} & 0 \\ 0 & 0 & \frac{\partial}{\partial z} \\ \frac{\partial}{\partial y} & \frac{\partial}{\partial x} & 0 \\ 0 & \frac{\partial}{\partial z} & \frac{\partial}{\partial y} \\ \frac{\partial}{\partial z} & 0 & \frac{\partial}{\partial x} \end{bmatrix} \cdot \underline{u} \tag{19}$$

with the shear γ. Neglecting initial strain and tension the correlation between strain $\underline{\epsilon}$ and tension $\underline{\sigma}$ is given by

$$\underline{\sigma} = \underline{H} \cdot \underline{\epsilon} = (\ \sigma_x\ \sigma_y\ \sigma_z\ \tau_{xy}\ \tau_{yz}\ \tau_{zx}\ )^T \tag{20}$$

where $\underline{H}$ is Hooke's matrix and τ the shear stress. The entries of $\underline{H}$ are defined by Young's modulus E and Poisson's ratio ν of the corresponding material. For the case of isotropic and homogenous bodies, $\underline{H}$ reads

$$\underline{H} = \frac{E(1-\nu)}{(1+\nu)(1-2\nu)} \cdot \begin{bmatrix} 1 & \frac{\nu}{1-\nu} & \frac{\nu}{1-\nu} & 0 & 0 & 0 \\ \frac{\nu}{1-\nu} & 1 & \frac{\nu}{1-\nu} & 0 & 0 & 0 \\ \frac{\nu}{1-\nu} & \frac{\nu}{1-\nu} & 1 & 0 & 0 & 0 \\ 0 & 0 & 0 & \frac{1-2\nu}{2(1-\nu)} & 0 & 0 \\ 0 & 0 & 0 & 0 & \frac{1-2\nu}{2(1-\nu)} & 0 \\ 0 & 0 & 0 & 0 & 0 & \frac{1-2\nu}{2(1-\nu)} \end{bmatrix}. \tag{21}$$

IV. Model Adaption

In a next step, the simple numerical model is replaced, applying the entire machine as shown in Fig. 3. In order to compare the results of both the analytical and numerical model, the analytical from Fig. 1 is reapplied for the housing considering the housing's dimensions. For this, the deformation of the stator on the outer radius R_a is sampled, depending on the number of spiral-steel springs (Fig. 4). The sampling can either be performed with the FE model or the analytical model. With the deformation samples the force excitation of the housing is calculated using Hooke's law in scalar form

$$\sigma = E \cdot \epsilon \qquad \epsilon = \frac{\Delta l}{l}. \tag{22}$$

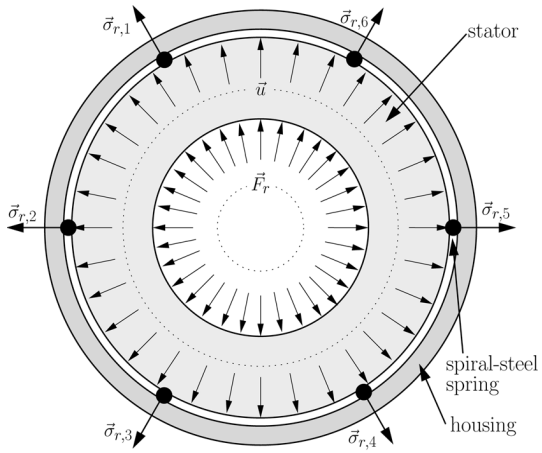

Fig. 4. Sampling of the stator deformation at location of springs.

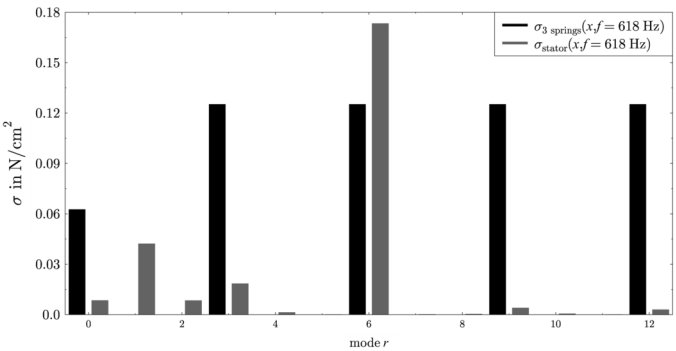

Fig. 5. Aliasing effect changing the exciting modes on the housing.

$l = h$ is the height of the stator yoke and Δl the magnitude of the deformation at the location of the spiral-steel spring.

After sampling, σ is transformed to the space domain providing the resulting modes of force excitation $r(\sigma)$. Due to the sampling, aliasing appears [5], depending on the original mode number. Fig. 5 shows the sampling and resulting mode numbers for $f = 618$ Hz exemplarily. The stator deformation shows a strong sixth mode. For three spiral-steel springs, the most significant mode numbers are $r = 0$ and 3.

V. Results

At first, the results of the analytical and numerical models without housing are compared (simple models). The deforma-

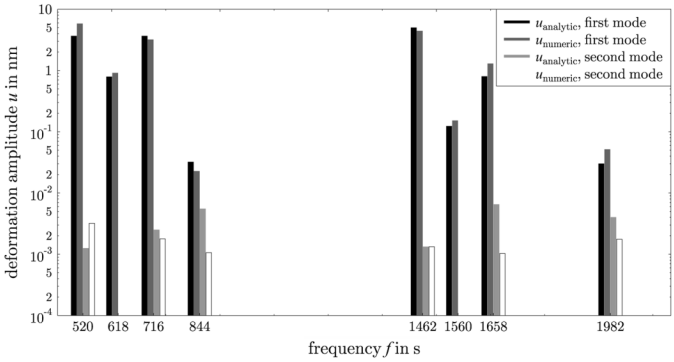

Fig. 6. Comparison of deformation magnitudes for models without housing.

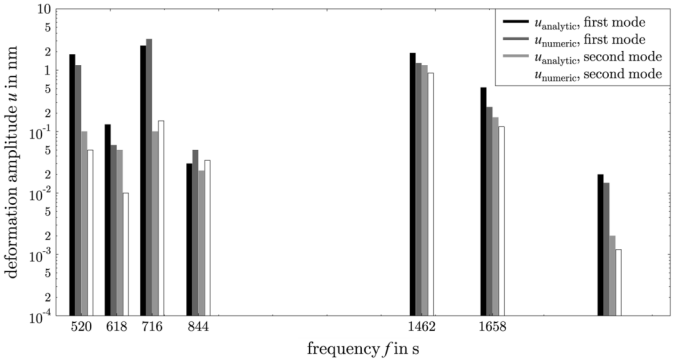

Fig. 7. Comparison of deformation magnitudes for models with housing.

tion modes r are analyzed seperately. By this, the impact of the mode number can be studied as well. Resuming the deformation values for some selected frequencies, Fig. 6 shows, that in the case of two modes with small mode numbers $(r \leq 10)$ of the exciting surface-force density the lower mode number has a significantly higher impact in any case. At $f = 844$ Hz for example, the mode numbers $r = 4$ and 8 occur. The latter having the higher force magnitude. Nevertheless, $r = 4$ reaches the higher deformation magnitude by a factor of 5.8. In general, if two modes appear the higher can be neglected. The only exception is the case of $r = 0$, which might produce lower deformation than $r = 1$ and 2. Next to this, Fig. 6 also states the very good accordance of the analytical and numerical models. Since the analytical model has been verified in general [1] the numerical model is stated to be reliable, providing good results.

Finally, the deformation is calculated for the machine model with the entire structure (Fig. 3) and applying the method described before (Fig. 4). In doing so, the impact of different stator-to-housing couplings is analyzed. Three models are studied: a model each with three and six spiral-steel springs and one with a shrinked stator which is equivalent to an infinite number of springs. Fig. 7 resumes the comparison of the analytical and numerical models with six springs.

Two effects can be stated. The first is that the housing increasing the stiffness of the machine as an additional mass, i.e., the height of the cylinder ring increases (Fig. 1), reduces the maximal deformation values. On the other hand, the aliasing (Fig. 5) results in smaller and additional mode numbers producing higher deformation. Both effects are detected in Fig. 7. For example $f = 844$ Hz shows higher deformation values for the model with housing and six springs. This is due to the fact that the original mode number $r = 8$ is transmitted to $r = 1$ and 2. For $f = 520$ Hz the maximal deformation reached at mode $r = 2$ is reduced by more than 50%.

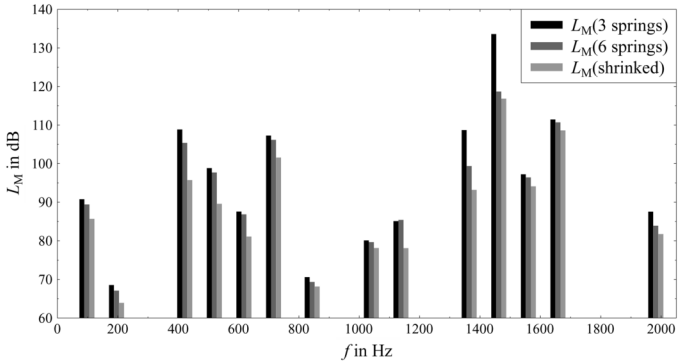

Fig. 8. Comparison of different stator-to-housing couplings.

Fig. 8 shows the comparison of the three different stator-to-housing couplings applying the body-sound index L_M. It can be stated that for all analyzed frequencies the shrinked model results in lowest deformation and vibration. Therefore, this variant will produce the lowest noise radiation. The variant with three springs is worst and should be discarded.

VI. Conclusion

The presented paper resumes the analytical theory of [1] and verifies the introduced numerical structure-dynamic model. The analysis of the deformational modes shows that small mode numbers have the strongest impact by far. The obtained results show the great impact of the type of stator-to-housing coupling to the noise radiation of electrical machines. In the case of a well designed IM by means of electromagnetic behavior, an awkward coupling results in unacceptable noise radiation. For the studied IM it is suggested to either shrink the housing or use an adequate number of springs for mounting.

References

[1] H. Jordan, *Geräuscharme Elektromotoren*. Essen, Germany: Verlag W. Girardet, 1950.
[2] O. C. Zienkiewicz and R. L. Taylor, *The Finite Element Method*. London, U.K.: McGraw-Hill, 1989.
[3] L. Vandevelde, J. J. C. Gyselinck, F. Bokose, and J. A. A. Melkebeek, "Vibrations of magnetic origin of switched reluctance motors," *COMPEL*, vol. 22, no. 4, pp. 1009–1020, Nov. 2003.
[4] C. Schlensok, D. van Riesen, T. Küest, and G. Henneberger, "Acoustic simulation of an induction machine with squirrel-cage rotor," *COMPEL*, vol. 25, no. 2, pp. 475–486, Mar. 2006.
[5] H. D. Lüke, *Signalübertragung*. Berlin, Germany: Springer-Verlag, 1999.

Manuscript received June 24, 2007. Corresponding author: C. Schlensok (e-mail: Christoph.Schlensok@boschrexroth.de).